J. Fluid Mech. (1994), *vol.* 272, *pp.* 21–44

The solidification of buoyancy-driven flow in a flexible-walled channel. Part 1. Constant-volume release

By JOHN R. LISTER

Institute of Theoretical Geophysics, Department of Applied Mathematics and Theoretical Physics, University of Cambridge, Silver Street, Cambridge CB3 9EW, UK

(Received 9 March 1993 and in revised form 24 January 1994)

The solidification of hot fluid flowing in a thin buoyancy-driven layer between cold solid boundaries is analysed in a series of two papers. As an approximation to flow in a crack in a weakly elastic solid or to free-surface flow beneath a thin solidified crust, the boundaries are considered to be flexible and to exert negligible resistance to lateral deformation. The resultant equations of continuity and motion reduce to a kinematic-wave equation with a loss term corresponding to the accumulation of solidified material at the boundaries. The Stefan problem for the solidification is coupled back to the flow through the advection of heat by the fluid, which competes with lateral heat loss by conduction to the solid. Heat and mass conservation are used to derive boundary conditions at the propagating nose of the flow. In this paper the two-dimensional flow produced by a line release of a given volume of fluid is investigated. It is shown that at short times the flow solidifies completely only near the point of release where the flow is thinnest, at later times complete solidification also occurs near the nose of the flow where the cooling rates are greatest and, eventually, the flow is completely solidified along its depth. Some transient melting of the boundaries can also occur if the fluid is initially above its solidification temperature. The dimensionless equations are parameterized only in terms of a Stefan number S and a dimensionless solidification temperature Θ. Asymptotic solutions for the flow at short times and near the source are derived by perturbation series and similarity arguments. The general evolution of the flow is calculated numerically, and the scaled time to final solidification, the length and the thickness of the solidified product are determined as functions of S and Θ. The theoretical solutions provide simple models of the release of a pulse of magma into a fissure in the Earth's lithosphere or of lava flow on the flanks of a volcano after a brief eruption. Other geological events are better modelled as flows fed by a continual supply of hot fluid. The solidification of such flows will be investigated in Part 2.

1. Introduction

It is of importance to those living in the shadow of an active volcano to know whether lava from an eruption on the volcano's flanks will cool, solidify and come to rest before it engulfs their homes. Similarly, geologists and volcanologists wish to understand in which circumstances molten rock, or magma, in the Earth's interior can penetrate the solid surface layers of the Earth to initiate an eruption. These cases provide examples of the more general question: how far can a hot fluid flow into cold surroundings before it solidifies and flow ceases?

In these two papers we investigate this problem, giving particular attention to the form it takes for the transport of magma through fissures, or dykes, in the Earth's lithosphere. Dykes are fluid-driven fractures, which propagate through the surrounding brittle rock owing to the injection of magma from a source region or reservoir (Pollard 1987). Dykes are pervasive through the Earth's crust, which suggests that magma-driven fracture is the dominant mechanism for the transport of magma towards the surface. Observations of seismicity associated with the advancing crack tip (Aki, Fehler & Das 1977; Einarsson & Brandsdóttir 1980; Shaw 1980) and of the size of rock fragments carried by the flow (Spera 1980; Pasteris 1984) indicate that propagation rates are of order a few metres per second, and the effectiveness of magma fracture as a transport mechanism is often linked to this rapid propagation since it allows transport for large distances with little solidification.

Magmas generated in the Earth's mantle, some tens or hundreds of kilometres below the surface, rise to accumulate at the base of the colder brittle lithosphere. Episodically, the accumulated magma is tapped as the stress builds up and a new dyke is initiated. Owing to the buoyancy of the magma relative to the surrounding country rock, the primary direction of propagation is upwards. A full physical description of the vertical propagation would thus involve the interacting effects of buoyancy, viscous flow, fracture and elastic deformation, heat transfer and solidification. Previous studies have concentrated on simplified combinations of the ingredients in this complicated process.

Early mechanical studies of dykes (e.g. Weertman 1971; Secor & Pollard 1975; Pollard 1976; Pollard & Holzhausen 1979) concentrated on solutions for the equilibrium shape of a stationary fluid-filled crack. These solutions may be relevant to the shape of exposed igneous intrusions if solidification takes place after propagation has ceased and the magma has come to rest. However, propagation is a dynamic process and scaling estimates of the forces involved show that the dominant resistance to propagation is the viscous pressure drop rather than the resistance of the host rock to fracture (Spence & Turcotte 1985; Lister 1990*a*; Lister & Kerr 1991). One corollary of this result is that the rheological change on solidification is more likely to cause the cessation of flow than to follow it.

The scaling arguments also show that, for dykes of more than a few kilometres in vertical extent, the dominant driving force is buoyancy, which leads to a simple viscous–buoyancy balance. The pressures required to produce elastic deformation of the walls are much less than the available buoyancy forces (Lister 1990*a*, 1991), so such dykes should be thought of as flexible, rather than rigid-walled, conduits which dilate sufficiently to accommodate the flux arriving from below. These conclusions are confirmed in travelling-wave solutions for steady upward propagation of a two-dimensional crack fed by a continuous linear source (Spence, Sharp & Turcotte 1987; Lister 1990*b*); elastic stresses are found only to be significant in the vicinity of the crack tip, below which the crack width tends to a constant value prescribed by the viscous–buoyancy balance and by the fluid supply rate. Using this result to justify the neglect of the details near the crack tip, Spence & Turcotte (1990) derived simple solutions for propagation from a two-dimensional constant-volume release. A similar approximation will be used below in our analysis of the interaction between solidification and flow.

Thermodynamic studies of the effects of heat transfer and solidification in cooling dykes are reviewed by Delaney (1987). The usual approach (e.g. Fedotov 1978; Wilson & Head 1981; Turcotte & Schubert 1982; Spence & Turcotte 1985) is to calculate the heat transfer by using one-dimensional diffusional models, thus neglecting any effects of advection and assuming that the magma has already come to rest. Approximate

blocking criteria are obtained by inserting this static solidification time into a model of flow without solidification. Coupled solutions for solidification and flow in an established rigid-walled conduit (Delaney & Pollard 1982; Bruce & Huppert 1989, 1990) highlight the importance of advection in the solidification problem and allow blocking criteria to be established for this case. However, solutions for heat transfer in a propagating and deformable conduit have yet to be given.

This context provides the motivation for the present study. We investigate solidification within a fluid-driven propagating crack embedded in an elastic solid. In §2 it is argued that elastic resistance is negligible away from the crack tip and the problem is reduced to calculation of heat transfer in a thin buoyancy-driven layer of hot liquid between cold and freely deformable solid boundaries. Lubrication approximations are used in the equations of heat and mass transport. The flow is described by a kinematic-wave equation with a loss term associated with solidification at the boundaries of the flow. Heat transfer is described by one-dimensional diffusion into a semi-infinite domain in the solid and by the interaction between along-stream advection and cross-stream diffusion in the liquid. The two heat-transfer problems are coupled by a Stefan boundary condition, which determines the local rate of solidification. At the propagating nose of flow, which is represented by the frontal shock of the kinematic wave, conservation of heat and mass are used to derive boundary conditions consistent with the lubrication approximation.

In §§3 and 4 these equations are solved for the case of the two-dimensional flow produced by release of a given volume of fluid from a line source. For simplicity, the thermal properties of the fluid and solid are assumed to be equal. With a suitable non-dimensionalization, the system can be parameterized by a Stefan number $S = L/C_p(T_0 - T_\infty)$ and dimensionless temperature $\Theta = (T_L - T_\infty)/(T_0 - T_\infty)$, where T_0 and T_∞ are the initial temperatures of fluid and solid, T_L is the liquidus temperature, L is the latent heat and C_p the specific heat capacity. As described in §3, if the fluid is initially at its liquidus temperature ($\Theta = 1$) the thermal equations are greatly simplified and the remaining equations can be solved by a modified method of characteristics. Asymptotic solutions for short times and for the near-source region are used to complement a complete numerical solution. The more general case $\Theta \neq 1$ is analysed in §4 and the results discussed in §5.

The most geologically significant conclusion is that the flow is completely solidified after a finite distance and time of propagation, which are evaluated as functions of S and Θ. The shape of the final solidified product is also calculated. The analysis is easily adapted to viscous flow down a slope under a cooled, solidifying but flexible crust, as appropriate for lava flows (Fink & Griffiths 1990).

2. Derivation of model and scaling

Consider the release from a horizontal line source of incompressible fluid of density ρ_f into a crack embedded in an infinite elastic solid of greater density ρ_s. The buoyancy of the fluid drives upward propagation of a two-dimensional crack which, with a suitable choice of coordinates, occupies $|x| \leqslant h(z,t)$ for $0 \leqslant z \leqslant z_N(t)$, where x is the cross-stream coordinate, z the vertical coordinate, $z = 0$ the level of release, $z = z_N(t)$ the level of the propagating crack tip and h the half-width of the crack (figure 1).

Let the initial temperatures of the fluid and the solid be T_0 and T_∞ respectively and suppose that the melting temperature of the solid and the solidification temperature of the fluid are equal and denoted by T_L, where $T_\infty < T_L \leqslant T_0$. Thus the propagation of the crack brings hot fluid into contact with cold solid and solidification or melting occurs.

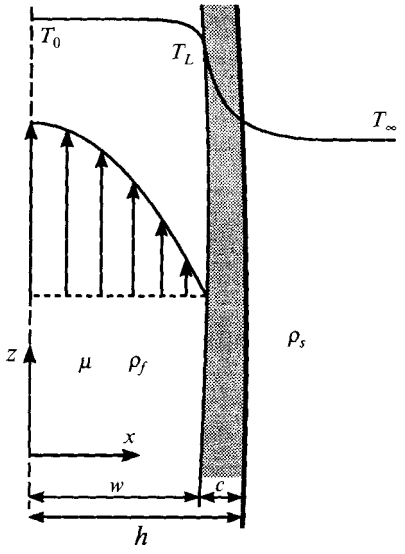

FIGURE 1. Definition sketch. A fluid of density ρ_f, viscosity μ, initial temperature T_0 and solidification temperature T_L is driven by buoyancy through a flexible conduit of width $2h(z,t)$ embedded in an elastic solid of density ρ_s and far-field temperature T_∞. The fluid solidifies to form a chill of width c, thus reducing the width of active flow to $2w$.

In consequence, we need to distinguish carefully between the total crack width $2h$, as defined by the lateral deformation of the original solid, and the active flow width $2w$, which is the thickness of the layer at the centre of the crack that is still fluid. The chill thickness $c = h-w$ is thus the thickness of the solidified layer at the edge of the flow (defined to be negative if melting has occurred). Whereas h is the natural variable to describe the elastic deformation, w and c are the natural variables to describe the flow and solidification problems.

2.1. *The fluid and solid mechanics*

Let the elastic response of the solid to deformation be described by shear modulus G and Poisson's ratio ν. The deviatoric elastic stress in the walls of the crack is thus given by

$$\sigma_{xx} = m\mathscr{H}\{\partial h/\partial z\} \tag{2.1}$$

(Muskhelishvili 1963), where $m = G/(1-\nu)$ and $\mathscr{H}\{\cdot\}$ denotes the Hilbert transform. The flow in the crack is driven by the gradient of the total effective pressure $p(z,t)$, which represents the sum of the buoyancy and elastic forces

$$p = -\Delta\rho g z - \sigma_{xx}, \tag{2.2}$$

where $\Delta\rho = \rho_s - \rho_f$. For simplicity, we assume that the effects of temperature on viscosity are dominated by the sudden increase on solidification and adopt a uniform fluid viscosity μ for $T > T_L$. (If necessary, numerical calculations with an empirical $\mu(T)$ would be possible.) If the crack is sufficiently narrow and the fluid sufficiently viscous then

$$\left|\frac{\rho_f w^3}{\mu^2}\frac{\partial w}{\partial z}\frac{\partial p}{\partial z}\right| \ll 1 \tag{2.3}$$

and the flow may be analysed by lubrication theory. The vertical fluid velocity is given

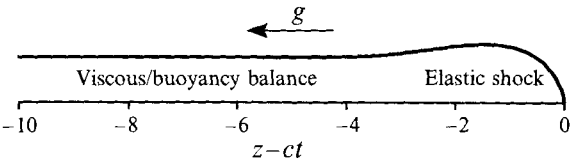

FIGURE 2. The dimensionless travelling-wave solution for buoyancy-driven fluid fracture with no solidification and negligible stress intensity (Lister 1990*b*). Elastic forces are only significant in the bulbous head of the wave; elsewhere there is a simple viscous/buoyancy balance.

by laminar Poiseuille flow driven by $\partial p/\partial z$ with $u_z = 0$ at $|x| = w$. The small lateral velocity is calculated from the local equation of continuity. Thus

$$\boldsymbol{u}(x, z, t) = \frac{1}{2\mu}\left\{\frac{\partial}{\partial z}\left((w^2 x - \tfrac{1}{3}x^3)\frac{\partial p}{\partial z}\right), (x^2 - w^2)\frac{\partial p}{\partial z}\right\} \quad (|x| \leqslant w). \tag{2.4}$$

The cross-sectionally averaged equation of continuity gives

$$\frac{\partial w}{\partial t} - \frac{1}{3\mu}\frac{\partial}{\partial z}\left(w^3 \frac{\partial p}{\partial z}\right) = -\frac{\partial c}{\partial t}, \tag{2.5}$$

where the solidification rate $\partial c/\partial t$ is determined by the thermal transport. It should be noted in the derivation of (2.5) that the lateral velocity u_x at $x = w$ is equal to the material velocity $\partial h/\partial t$ and not the velocity of the phase boundary $\partial w/\partial t$.

In the absence of solidification $w = h$ and so (2.1), (2.2) and (2.5) may be combined to yield

$$\frac{\partial w}{\partial t} + \frac{\Delta\rho g}{3\mu}\frac{\partial w^3}{\partial z} = -\frac{m}{3\mu}\frac{\partial}{\partial z}\left(w^3 \frac{\partial}{\partial z}\mathscr{H}\left\{\frac{\partial w}{\partial z}\right\}\right). \tag{2.6}$$

Equation (2.6) admits a family of travelling-wave solutions parameterized by the rate of propagation and the stress intensity ahead of the crack tip (Lister 1990*b*). The solutions exhibit a bulbous head in which all three terms of (2.6) are important, followed by a tail in which there is a simple viscous–buoyancy balance and elastic forces are negligible (figure 2). More generally, solutions of (2.6) may be considered as buoyancy-driven kinematic waves in which elastic forces only act locally to smooth the frontal shock over a vertical distance

$$z_e = O(mw/g\Delta\rho)^{1/2} \tag{2.7}$$

(Lister & Kerr 1991). If the vertical extent of the flow is much greater than z_e then the elastic term may be neglected and conservation of mass used to calculate the rate of propagation of any shocks (e.g. Spence & Turcotte 1990). We use this approximation in the analysis below, thus considering the walls of the crack to be perfectly flexible, but retaining the solidification term in (2.5).

2.2. *Thermal transport and solidification*

We suppose, for simplicity, that the thermal properties of the solid, the fluid and its solidified product are equal. Conservation of heat is represented by

$$\partial T/\partial t + \boldsymbol{u}\cdot\nabla T = \kappa\nabla^2 T, \tag{2.8}$$

where κ is the thermal diffusivity and $\boldsymbol{u}$ is given by (2.4) in the liquid region and by the

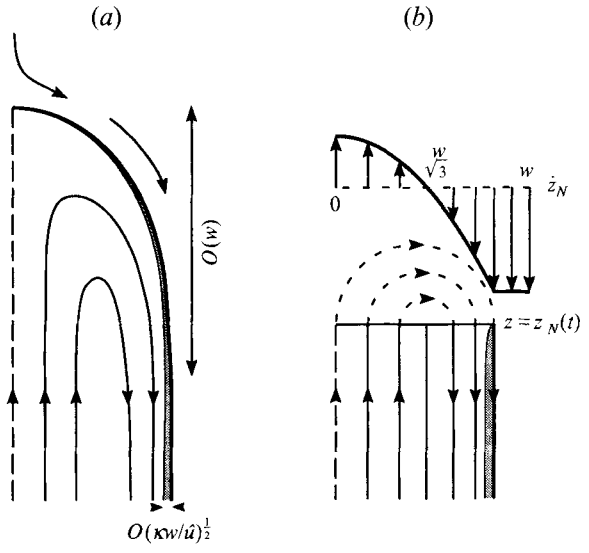

FIGURE 3. (*a*) The streamlines in the frame of reference moving with the nose are nearly parallel except within an $O(w)$ distance of the nose. Within this region the thermal boundary layer (stippled) is still very thin since $\hat{u}w/\kappa \gg 1$. (*b*) In the lubrication approximation the turn-round region is neglected and streamlines are identified in such a way as to conserve both heat and mass.

rate of deformation in the solid region. We are interested in cracks that propagate many times their own width before solidifying. Comparison of the solidification timescale $O(h^2/\kappa)$ with the advection timescale $O(h/\hat{u})$, where $\hat{u}$ is a typical velocity based on (2.4), shows that we require

$$\hat{u}h/\kappa \gg 1. \tag{2.9}$$

This condition leads to two simplifications in (2.8). Firstly, the cross-stream temperature gradients are much larger than the along-stream gradients and we may neglect the term $\kappa(\partial^2 T/\partial z^2)$ which corresponds to along-stream conduction. The simplified equation is hyperbolic in z and t and requires 'upstream' boundary conditions to be specified. Secondly, during solidification the heat from the fluid only has time to diffuse a distance $O(h)$ into the solid on either side of the crack. Since this is much less than the lengthscale $O(z_N)$ characteristic of the elastic deformation in the solid, we may approximate $\boldsymbol{u}$ in the solid by the rate of lateral displacement of the crack walls

$$\boldsymbol{u}(x,z,t) = \operatorname{sgn}(x)\left(\frac{\partial h}{\partial t},0\right) = \operatorname{sgn}(x)\left(\frac{\partial w}{\partial t}+\frac{\partial c}{\partial t},0\right) \quad (|x| \geqslant w). \tag{2.10}$$

A third simplification arising from (2.9) occurs in the thermal boundary conditions at the nose of the flow. Within the kinematic-wave approximation, the nose of the flow corresponds to a shock whose propagation rate may be shown by conservation of mass to be equal to the mean velocity in the Poiseuille profile just behind the shock (figure 3*b*). From (2.2) and (2.4) we find that

$$h_N \frac{\mathrm{d}z_N}{\mathrm{d}t} = \frac{\Delta\rho g}{3\mu} w_N^3, \tag{2.11}$$

where $h_N = h(z_N)$ and $w_N = w(z_N)$. In the frame of reference moving with the nose, the actual streamlines will be as shown schematically in figure 3(*a*). Rapidly moving fluid in the central region of the flow catches up with the nose, is turned round within an $O(w)$ distance of the nose, deposited near the stationary crack walls and then left behind again. In using the kinematic-wave approximation, we have argued that we may neglect the details of the flow in the turn-round region in the immediate vicinity of the nose and consider the streamlines to be as shown in figure 3(*b*). We now make a similar approximation for the thermal transport at the nose. We neglect cross-stream conduction in the turn-round region since the thickness $O(\kappa w/\hat{u})^{1/2}$ of the thermal boundary layer at the exit of the turn-round region is much less than w by (2.9). Thus we identify the temperature on the incoming streamlines in $w_N/\sqrt{3} \leqslant |x| \leqslant w_N$ with the temperature on the corresponding outgoing streamline in $|x| \leqslant w_N/\sqrt{3}$. This boundary condition is consistent with the hyperbolic nature of (2.8) after the neglect of along-stream conduction. We also find that $h_N = w_N$.

At the solidification boundary the temperature must be equal to the solidification temperature and the release of latent heat is balanced by a discontinuity in the conductive heat flux. Hence, we obtain the thermal boundary conditions

$$T = T_L \quad (|x| = w), \tag{2.12}$$

$$L\frac{\partial c}{\partial t} + C_p \kappa \left[\frac{\partial T}{\partial x}\right]_-^+ = 0, \tag{2.13}$$

where $[\cdot]_-^+$ denotes the difference between values at $x = w_+$ and $x = w_-$. Further boundary conditions are provided by the initial temperatures of fluid and solid and the temperature at infinity.

2.3. *The scaled system of equations*

Before summarizing the system of equations to be solved, it is convenient to define dimensionless variables in terms of a reference width $\hat{h}$. We define a dimensionless temperature by

$$\theta = \frac{T - T_0}{T_\infty - T_0} \tag{2.14}$$

and non-dimensionalize the remaining variables with respect to the scales

$$\hat{x} = \hat{h}, \quad \hat{u}_z = \frac{g\Delta\rho\hat{h}^2}{\mu}, \quad \hat{z} = \frac{\hat{u}_z\hat{h}^2}{\kappa}, \quad \hat{u}_x = \frac{\hat{u}_z\hat{h}}{\hat{z}}, \quad \hat{t} = \frac{\hat{z}}{\hat{u}_z} = \frac{\hat{h}^2}{\kappa}. \tag{2.15}$$

Among the associated dimensionless groups we may identify a Péclet number, modified Reynolds number and elastic parameter by

$$Pe = \hat{u}_z\hat{h}/\kappa = g\Delta\rho\hat{h}^3/\kappa\mu, \tag{2.16a}$$

$$Re = (\rho_f \hat{u}_z \hat{h}/\mu)(\hat{h}/\hat{z}) = \rho_f \kappa/\mu, \tag{2.16b}$$

$$M = (m/g\Delta\rho\hat{h})^{1/2}. \tag{2.16c}$$

The use of linear elasticity in (2.1) requires $M \gg 1$, the use of lubrication theory in (2.4) requires $Re \ll 1$, the neglect of along-stream conduction in (2.8) requires $Pe \gg 1$ and the neglect of the elastic pressure in (2.2) requires $z_e \ll \hat{z}$ or, equivalently, $M \ll Pe$. These conditions are satisfied for a range of geologically reasonable parameters.

When expressed in the new dimensionless variables, the simplified forms of (2.4), (2.5), (2.8) and (2.10)–(2.13) are

$$\theta_t + \boldsymbol{u}\cdot\nabla\theta = \theta_{xx}, \tag{2.17}$$

$$\boldsymbol{u} = (-ww_z x, \tfrac{1}{2}(w^2 - x^2)) \quad (0 \leqslant x \leqslant w), \tag{2.18a}$$

$$\boldsymbol{u} = (-w^2 w_z, 0) \quad (w \leqslant x), \tag{2.18b}$$

$$w_t + w^2 w_z + c_t = 0 \quad (0 < z < z_N), \tag{2.19}$$

$$Sc_t + [\theta_x]^+_- = 0 \quad (w > 0), \tag{2.20}$$

$$\theta(w, z, t) = \Theta, \tag{2.21}$$

$$\mathrm{d}z_N/\mathrm{d}t = \tfrac{1}{3}w_N^2, \tag{2.22}$$

$$c(z_N) = 0, \tag{2.23}$$

together with symmetrical conditions in $x < 0$, where

$$S = \frac{L}{C_p(T_0 - T_\infty)}, \tag{2.24}$$

$$\Theta = \frac{T_L - T_\infty}{T_0 - T_\infty}, \tag{2.25}$$

and subscripts t, x and z denote partial derivatives. The initial and far-field temperature in the solid is $\theta = 0$ and the initial temperature in the fluid is $\theta = 1$.

The stream function in the frame of reference of the nose of the flow is proportional to $w^2x - x^3$. By considering the solutions of $w^2x - x^3 = w^2\tilde{x} - \tilde{x}^3$, we deduce that the incoming streamline at (x, z_N), where $w_N/\sqrt{3} < x < w_N$, corresponds to the outgoing streamline at $(\tilde{x}, z_N)$, where $\tilde{x}(x)$ is the positive root of

$$\tilde{x}^2 + x\tilde{x} + x^2 = w_N^2. \tag{2.26}$$

Thus the thermal boundary conditions to be imposed on (2.17) at $z = z_N$ are

$$\theta(x, z_N, t) = \theta(\tilde{x}(x), z_N, t) \quad (w_N/\sqrt{3} < x < w_N), \tag{2.27a}$$

$$\theta(x, z_N, t) = 0 \quad (w_N < x), \tag{2.27b}$$

together with symmetry in $x = 0$.

Equation (2.19) requires $w(0, t)$ or, equivalently, the source flux to be specified. The case of continual release is analysed in Part 2 (Lister 1994). In the following sections, however, we analyse the case of an instantaneous point release of a fixed (two-dimensional) volume Q at $t = 0$ for which $w(0, t) = 0$ when $t > 0$. The dimensional volume of such a release may be scaled out of the problem by use of the reference length

$$\hat{h} = (3Q\mu\kappa/4g\Delta\rho)^{1/5}, \tag{2.28}$$

to obtain the dimensionless boundary conditions

$$\lim_{t\to 0_+} \int_0^{z_N(t)} 2w(z, t)\,\mathrm{d}z = \tfrac{4}{3}, \quad \lim_{t\to 0_+} z_N(t) = 0. \tag{2.29}$$

As a preliminary to solving the full system of dimensionless equations, it is helpful

to consider a simple solution in which solidification is neglected, corresponding to either of the limits $S \to \infty$ or $t \to 0$. In this case, we need only to solve

$$w_t + w^2 w_z = 0 \quad (0 < z < z_N) \tag{2.30}$$

subject to (2.22) and (2.29). The solution is readily calculated by the method of characteristics to be

$$w(z,t) = (z/t)^{1/2}, \quad z_N = t^{1/3} \tag{2.31a, b}$$

(e.g. Huppert 1982; Spence & Turcotte 1990).

3. Fluid initially at its liquidus temperature: $\Theta = 1$

The solution of (2.17)–(2.29) is greatly simplified if the fluid is initially at its liquidus temperature, corresponding to $\Theta = 1$. The initial fluid temperature is thus equal to the boundary temperature imposed by (2.21) for $t > 0$, and hence the solution of (2.17) in the fluid region is trivially

$$\theta = 1 \quad (|x| \leqslant w). \tag{3.1}$$

We note that, since the fluid temperature remains constant when initially on its liquidus, it is possible to extend the analysis to turbulent flows without need for an empirical turbulent heat-transfer function; solutions for turbulent flows are derived in Appendix A.

The velocity field in the solid is a simple lateral displacement, and use of the coordinate transformation $x' = x - w - c$ together with (2.18*b*) and (2.19) reduces (2.17) to

$$\theta_t = \theta_{x'x'} \quad (x' \geqslant -c). \tag{3.2}$$

It follows that the thermal problem posed by (2.20), (2.21), (2.23), (2.27), (3.1) and (3.2) is equivalent to one-dimensional solidification of a liquid placed in contact with a semi-infinite cold solid at time $t = t_N(z)$, where $t_N(z)$ is the time at which the nose of the flow reaches z. While w remains positive, the solution is given by

$$\theta = \frac{\operatorname{erfc}\left(\dfrac{x'}{2(t-t_N)^{1/2}}\right)}{\operatorname{erfc}(-\lambda)} \quad (x' \geqslant -c, t > t_N), \tag{3.3a}$$

$$c = 2\lambda(t-t_N)^{1/2} \qquad (t > t_N) \tag{3.3b}$$

(Carslaw & Jaeger 1959), where $\lambda(S)$ is the root of

$$S\pi^{1/2}\lambda\, \mathrm{e}^{\lambda^2} \operatorname{erfc}(-\lambda) = 1. \tag{3.3c}$$

This solves the thermal problem in terms of the function $t_N(z)$, which is as yet unknown.

Substitution of (3.3*b*) into (2.19) yields the modified kinematic-wave equation

$$w_t + w^2 w_z = -\lambda[t - t_N(z)]^{1/2} \quad (w > 0), \tag{3.4}$$

in which the loss term on the right-hand side corresponds to solidification and t_N is found from (2.22). The dependence on λ can be scaled out by defining

$$Z = z\lambda^{2/5}, \quad W = w\lambda^{-2/5}, \quad T = t\lambda^{6/5} \tag{3.5}$$

but for the moment we retain it as a convenient expansion parameter in the following section.

3.1. *Short-time expansion*

In the limit $\lambda \to 0$ the solution of (3.4) must tend to the solution (2.31) without solidification. This suggests that we can use the method of characteristics to seek a perturbation expansion for the limit of slow solidification or, equivalently, of short times. We label characteristics $z(t;\phi)$ by $\phi = \lim_{t\to 0} w^2$, and write (3.4) as

$$(\partial z/\partial t)_\phi = w^2, \tag{3.6a}$$

$$(\partial w/\partial t)_\phi = -\lambda/[t - t_N(z)]^{1/2} \quad (w > 0), \tag{3.6b}$$

$$z(0;\phi) = 0, \quad w(0;\phi) = \phi^{1/2}. \tag{3.6c, d}$$

The solution is expanded as

$$z(t;\phi) = z_0 + \lambda z_1 + O(\lambda^2), \quad w(t;\phi) = w_0(t;\phi) + \lambda w_1(t;\phi) + O(\lambda^2), \tag{3.7a, b}$$

$$t_N[z(t;\phi)] = t_0(z) + \lambda t_1(z) + O(\lambda^2). \tag{3.7c}$$

The leading-order solution, equivalent to (2.31), is clearly

$$z_0 = \phi t, \quad w_0 = \phi^{1/2}, \quad t_0 = z^3 = (\phi t)^3. \tag{3.8a–c}$$

Substituting into (3.6) at $O(\lambda)$, we find that

$$w_{1t} = -1/(t - \phi^3 t^3)^{1/2} \quad z_{1t} = 2 w_0 w_1. \tag{3.9}$$

By integration and use of the identity $w_1 = (w_1 t)_t - w_{1t} t$, we obtain

$$w_1(t;\phi) = -\int_0^t \frac{\mathrm{d}\tau}{(\tau - \phi^3\tau^3)^{1/2}}, \tag{3.10a}$$

$$z_1(t;\phi) = 2\phi^{1/2} \int_0^t \frac{(\tau - t)\,\mathrm{d}\tau}{(\tau - \phi^3\tau^3)^{1/2}}, \tag{3.10b}$$

where the integrals may be evaluated if required in terms of elliptic functions (Gradshteyn & Ryzhik 1980, equations 3.131.5 and 3.132.4). In order to solve (2.22) for the $O(\lambda)$ correction to the rate of propagation of the nose, we need to re-express w as a function of z and t and find $w(z_N, t)$. Accordingly, we define

$$w(z,t) = \omega_0(z,t) + \lambda\omega_1(z,t) + O(\lambda^2). \tag{3.11}$$

Comparison with (3.7) and (3.8) shows that

$$\omega_0(z,t) = w_0(t; z/t) = (z/t)^{1/2}, \tag{3.12a}$$

$$\omega_1(z,t) = w_1(t; z/t) - \frac{z_1(t; z/t)}{2(tz)^{1/2}} = -\int_0^t \frac{\tau}{t} \frac{\mathrm{d}\tau}{(\tau - z^3\tau^3/t^3)^{1/2}}. \tag{3.12b}$$

We use (3.8*c*) to write (2.22) in the form

$$3\frac{\mathrm{d}z_N}{\mathrm{d}t} = \omega_0^2(z_N, t)\left(1 + 2\lambda\frac{\omega_1(t^{1/3}, t)}{\omega_0(t^{1/3}, t)}\right) + O(\lambda^2), \tag{3.13}$$

which may readily be integrated to obtain

$$z_N = t^{1/3}(1 - \tfrac{2}{5}\lambda \mathrm{B}(\tfrac{3}{4}, \tfrac{1}{2})\, t^{5/6}) + O(\lambda^2), \tag{3.14}$$

where B denotes the beta function

$$\mathrm{B}(a,b) = \int_0^1 v^{a-1}(1-v)^{b-1}\,\mathrm{d}v = \frac{\Gamma(a)\,\Gamma(b)}{\Gamma(a+b)} \tag{3.15}$$

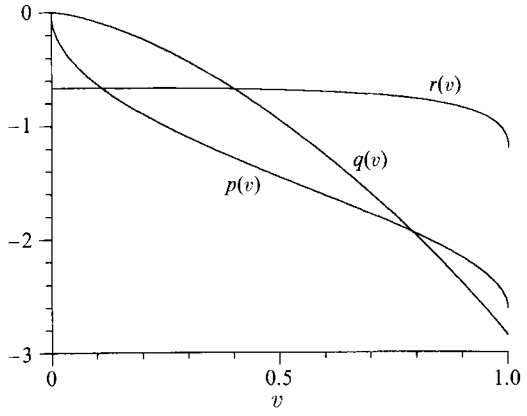

FIGURE 4. The first-order perturbations: $w_1(t;\phi) = \phi^{-3/4}p(\phi^{3/2}t)$, $z_1(t;\phi) = \phi^{-7/4}q(\phi^{3/2}t)$ and $\omega_1(z,t) = t^{1/2}r(z^3/t)$, where p, q and r are as shown.

and $\mathrm{B}(\frac{3}{4},\frac{1}{2}) \approx 2.396$. Hence $t_1 = \frac{6}{5}\mathrm{B}(\frac{3}{4},\frac{1}{2})z^{11/2}$, which completes the solution to this order. The first-order perturbations w_1, ω_1 and z_1 are shown in figure 4. Higher-order corrections can be calculated as described in Appendix B.

The initial effects of solidification can be seen in the first-order solution. From (3.13) the fluid width is everywhere less than the non-solidifying solution (though the total width h is greater) and from (3.14) the rate of propagation is decreased. Though we have solved the equations by expansion in the limit $\lambda \to 0$, the solution can also be considered as an early-time expansion in the limit $t \to 0$. As might be expected from (3.5), these viewpoints can be combined into the asymptotic requirement $T = \lambda^{5/6}t \ll 1$. However, the solution (3.12) is not uniformly valid for all z since $\omega_0 \propto z^{1/2}$ and ω_1 tends to a constant as $z \to 0$ with t fixed. We therefore also seek an asymptotic solution to (3.4) in the limit $z \to 0$.

3.2. *Near-source similarity solution*

Clearly $t_N(z) \to 0$ as $z \to 0$. Hence, for sufficiently small z we can assume that $t \gg t_N(z)$ and approximate (3.6*b*) by

$$(\partial W/\partial T)_\phi \sim -T^{-1/2} \quad (W > 0). \tag{3.16}$$

(Henceforth, we will use the rescaled variables defined by (3.5).) Equations (3.16) and (3.6*a*) may then be integrated to obtain

$$W \sim \phi^{1/2} - 2T^{1/2} \quad (T < \tfrac{1}{4}\phi), \tag{3.17a}$$

$$Z \sim \phi T + \tfrac{8}{3}\phi^{1/2}T^{3/2} + 2T^2. \tag{3.17b}$$

We eliminate ϕ and find a self-similar solution of the form

$$W = T^{1/2}F(Z/T^2), \tag{3.18a}$$

where

$$F(\eta) = (\eta - \tfrac{2}{9})^{1/2} - \tfrac{2}{3} \quad (\eta > \tfrac{2}{3}), \tag{3.18b}$$

$$= 0 \qquad\qquad (\eta < \tfrac{2}{3}). \tag{3.18c}$$

Hence, complete solidification begins near the source and occupies a zone

$$0 \leqslant Z \leqslant Z_S \sim \tfrac{2}{3}T^2. \tag{3.19}$$

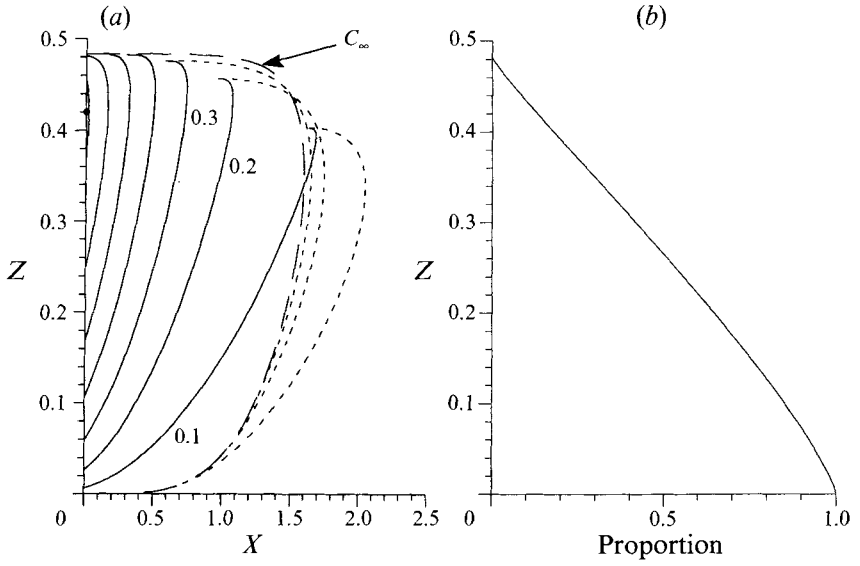

FIGURE 5. (*a*) The flow width (solid lines) obtained from (2.22) and (3.4) as a function of vertical distance Z at successive times $T = 0.1, 0.2, \ldots, 0.7$. The effects of solidification are strongest near the source where the flow is narrow and near the nose where the temperature gradients are steep. Propagation ceases at $T = 0.52$ and solidification is complete by $T = 0.72$ (●). Also shown is the deformation of the original solid at $T = 0.1$, 0.2 and 0.3 (dashed) and the final chill thickness $C_\infty = c\lambda^{-2/5}$ (long dashed). (*b*) The proportion $\frac{3}{2}\int_Z^{Z_{max}} C_\infty \, dZ$ of the initial fluid that reaches level Z. If a dyke reaches the Earth's surface then this will be the proportion of magma erupted.

For $T^2 \ll Z \ll T^{1/3}$ the solutions (3.12) and (3.17) are matched by the common asymptotic form

$$W \sim (Z/T)^{1/2} - \tfrac{2}{3}T^{1/2}. \tag{3.20}$$

3.3. *Numerical solution*

As described above, asymptotic methods have been used to determine the first effects of solidification on the propagating flow. The asymptotic results provide both starting conditions and accuracy tests for numerical integration of the full evolution of the flow. We observe first that, if we are given $T_N(Z)$, it is straightforward to integrate (3.6) using, for example, a fourth-order Runge–Kutta method. The function T_N is determined by the requirement that if a characteristic $Z(T;\phi)$ crosses the curve $T = T_N(Z)$ then the value of W obtained from (3.6) is related to dT_N/dZ by (2.22).

Suppose we know $T_N(Z)$ for $Z < Z_i$, that the characteristic reaching the nose at Z_i is ϕ_i and that the width at the nose is W_i. We extend this solution by the quadratic approximation to the Taylor series,

$$T_N(Z) = T_N(Z_i) + 3(Z - Z_i)/W_i^2 + \alpha_i(Z - Z_i)^2 \quad (Z > Z_i), \tag{3.21}$$

that is consistent with (2.22) at Z_i. The value of α_i is determined iteratively by requiring consistency between (2.22) and (3.21) at the intersection Z_{i+1} of the characteristic $\phi_{i+1} = \phi_i - \Delta\phi$ with the quadratic extension. By starting with the asymptotic form $T_N(Z) \sim Z^3 + \frac{6}{5}\mathrm{B}(\frac{3}{4}, \frac{1}{2})Z^{11/2}$ for $Z \leqslant Z_0$, where $Z_0 \ll 1$, and making successive extensions with small increments $\Delta\phi$, we can thus generate a numerical solution.

The flow and chill widths are shown at successive times in figure 5(*a*). At early times the flow width is qualitatively similar to the solution without solidification (2.31), but with small deviations described by the perturbation solution (3.12). Complete

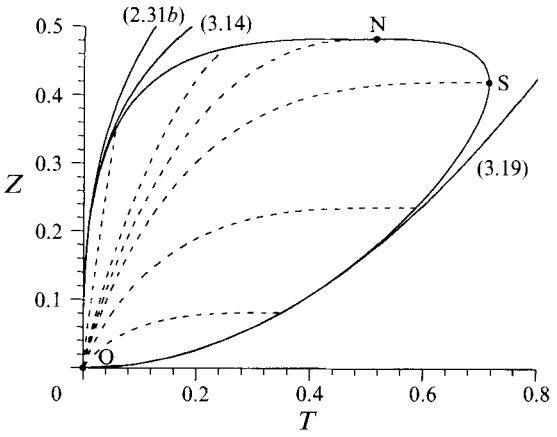

FIGURE 6. The figure shows (i) the propagation of the nose of a flow on its liquidus (ON, upper curve) together with the zeroth and first-order short-time asymptotic solutions (2.31*b*) and (3.14); (ii) the limits of the zones of complete solidification (OS and SN) together with the near-source asymptotic limit (3.19). Propagation ceases at N; solidification is complete at S. The solution was determined by a modified method of characteristics some of which are shown dashed.

solidification begins at the source of the flow and extends upward as described by (3.19). At larger times the rapid rates of solidification near the nose of the flow cause the width there to decrease sharply and at $T \approx 0.52$ and $Z \approx 0.48$ the nose of the flow also solidifies completely and propagation ceases. The remaining fluid continues to move slowly upwards, but solidification is now dominant and the zones of complete solidification extend from both nose and tail. The last part of the flow solidifies at $T \approx 0.72$ and $Z \approx 0.42$. For application to dykes that reach the Earth's surface it is interesting to note that if the flow is truncated at some level $Z < 0.48$ then only a proportion of the initial fluid reaches that level and erupts (figure 5*b*).

The positions of the nose and the zones of complete solidification are shown as functions of time in figure 6, together with some characteristic trajectories. Along the segment ON the width W satisfies the nose condition (2.22) and hence the slope of the characteristics is three times that of ON at intersections. Along the segments OS and SN the width is zero and hence the characteristics are horizontal. Owing to solidification, the characteristics do not cross after the nose is completely frozen, despite the possibility of nonlinear steepening and shock formation in a kinematic wave. The asymptotic results (3.14) and (3.19) for the positions of the nose of the flow and the zone of complete solidification are shown for comparison.

4. Fluid initially above its liquidus temperature: $\Theta < 1$

If the initial temperature of the fluid is greater than the liquidus temperature imposed at the phase boundary $x = w$ then temperature gradients develop in the fluid owing to the sidewall cooling. In this case, we must also consider the advection–diffusion equation (2.17) for the heat transport in the fluid and solution is much more difficult, both analytically and numerically, than for fluid initially at its liquidus temperature.

4.1. *Short-time expansion*

We may make some analytical progress by recognizing that the temperature contrasts at short times will be confined to thermal boundary layers near the stationary walls of the flow. We expect, therefore, that the effects of advection will initially be small, as can

be confirmed by scaling estimates. At leading order, solidification has no effect on the flow (cf. §3.1) and the scales of width, length and centreline velocity are given by $\hat{w} \sim t^{-1/3}$, $\hat{z} \sim t^{1/3}$ and $\hat{u} \sim t^{-2/3}$. The thickness of the thermal boundary layer grows diffusively and has width $\hat{\delta} \sim t^{1/2}$. Since $\hat{\delta} \ll \hat{w}$ for $t \ll 1$, the thermal boundary layer is embedded in the shear flow at the edge of the Poiseuille profile and is, therefore, only subject to velocities of order $\hat{u}\hat{\delta}/\hat{w}$. The ratio of advection to diffusion in (2.17) is thus

$$u\theta_z/\theta_{xx} \sim (\hat{u}\hat{\delta}/\hat{w})\,\hat{\delta}^2/\hat{z} \sim t^{5/6} \ll 1. \tag{4.1}$$

Hence, advection induces an $O(t^{5/6})$ correction to the rate of solidification as calculated only from cross-stream diffusion and, as in §3, the leading-order effect of solidification on the flow is itself an $O(t^{5/6})$ correction to the loss-less kinematic wave. Thus the effects of advection do not appear until second order in an expansion in powers of $t^{5/6}$ and we may use the techniques of §3.1.

The transformation $x' = x - w - c$ now gives

$$\theta_t = \theta_{x'x'} + O(t^{5/6}) \quad (x' \leqslant O(t^{1/2})). \tag{4.2}$$

Near the source $w \to 0$ and we will have to treat this region separately in the following section. Away from the source, however, $w \gg \delta \sim O(t^{1/2})$ and the growth of c near $x' = 0$ may be calculated by treating the fluid as semi-infinite. One-dimensional solidification of a semi-infinite fluid of initial temperature $\theta = 1$ placed in contact with a semi-infinite solid of initial temperature $\theta = 0$ at $t = t_N$ is described by

$$\theta = \frac{\Theta \operatorname{erfc}\left(\dfrac{x'}{2(t-t_N)^{1/2}}\right)}{\operatorname{erfc}(-\lambda)} \qquad (x' \geqslant -c,\, t > t_N), \tag{4.3a}$$

$$\theta = 1 - \frac{(1-\Theta)\operatorname{erfc}\left(\dfrac{-x'}{2(t-t_N)^{1/2}}\right)}{\operatorname{erfc}\lambda} \qquad (x' \leqslant -c,\, t > t_N), \tag{4.3b}$$

$$c = 2\lambda(t-t_N)^{1/2} \qquad (t > t_N) \tag{4.3c}$$

(Carslaw & Jaeger 1959), where $\lambda(S, \Theta)$ is the root of

$$S\pi^{1/2}\lambda\, \mathrm{e}^{\lambda^2} = \frac{\Theta}{\operatorname{erfc}(-\lambda)} - \frac{1-\Theta}{\operatorname{erfc}\lambda}. \tag{4.3d}$$

If $\Theta < \frac{1}{2}$ then $\lambda < 0$ and melting rather than solidification will occur initially.

Once λ has been found, the propagation and width of the flow are described by the perturbation solution (3.7)–(3.8) and (3.10)–(3.14), which is accurate to $O(\lambda t^{5/6})$. Calculation of the $O(\lambda^2 t^{5/3})$ corrections would involve the advection of the error-function temperature profile by the leading-order velocity field. Advection must also be taken into account near the source where the width of the flow is comparable to the thickness of the thermal boundary layers.

4.2. *Near-source similarity solution*

Near the origin we neglect $t_N(z)$ in comparison with t and expect that the lateral scale will be simply proportional to the diffusive scale $t^{1/2}$. Accordingly, we look for a similarity solution of the form

$$\theta(x, z, t) = \vartheta(\xi, \zeta), \quad w = t^{1/2} f(\zeta), \tag{4.4}$$

where

$$\xi = x/t^{1/2}, \quad \zeta = z/t^2. \tag{4.5}$$

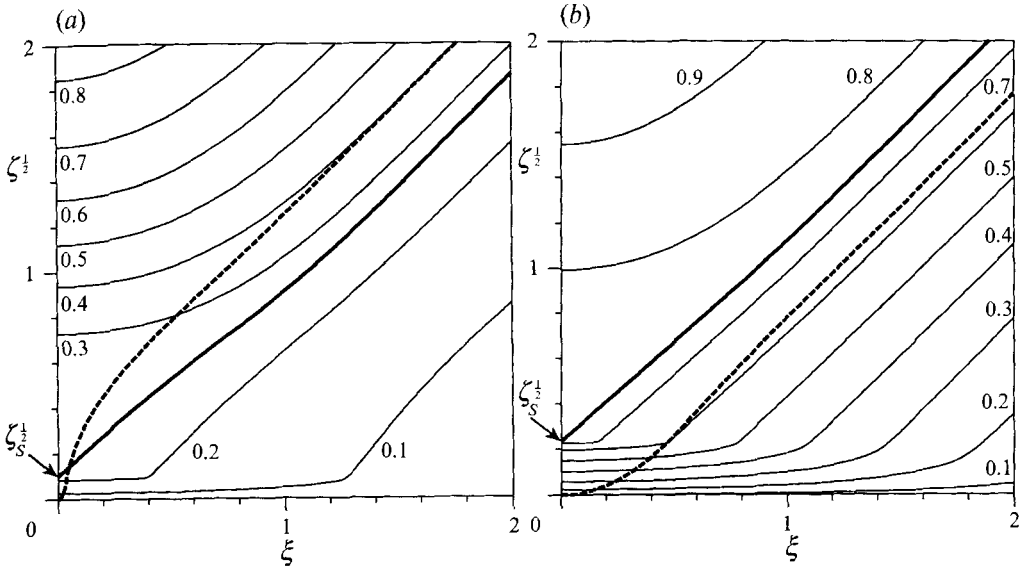

FIGURE 7. Contours of temperature ϑ in the near-source similarity solution (4.6) for $S = 1$, shown in $(\xi, \zeta^{1/2})$ space in order to exhibit the asymptotic structure (4.7). The edge of the flow (bold) corresponds to the isotherm $\vartheta = \Theta$; the extent of the deformation $h = w + c$ is shown dashed. Solidification is complete in $\zeta < \zeta_S$; far from the origin the flow is solidifying if $\Theta > \frac{1}{2}$ and melting otherwise. (*a*) $\Theta = 0.25$; (*b*) $\Theta = 0.75$.

In terms of the new variables, (2.17)–(2.20) may be written

$$(f^2 - 2\zeta) f' + \tfrac{1}{2} f = S^{-1}[\vartheta_\xi]_-^+, \tag{4.6a}$$

$$\{\tfrac{1}{2}(f^2 - \xi^2) - 2\zeta\}\,\vartheta_\zeta - (ff' + \tfrac{1}{2})\,\xi\vartheta_\xi = \vartheta_{\xi\xi} \quad (|\xi| \leqslant f), \tag{4.6b}$$

$$-2\zeta\vartheta_\zeta - (f^2 f' + \tfrac{1}{2}\xi)\,\vartheta_\xi = \vartheta_{\xi\xi} \quad (|\xi| \geqslant f), \tag{4.6c}$$

where $f' = \mathrm{d}f/\mathrm{d}\zeta$.

Equation (4.6*c*) is parabolic with $-\zeta$ as the time-like direction. Equation (4.6*b*) is also parabolic in ζ and, provided $f < 2\zeta^{1/2}$, $-\zeta$ is the time-like direction throughout the flow. It follows that we need boundary conditions on ϑ and f as $\zeta \to \infty$. These are provided by the asymptotic form of the short-time solution (3.12) and (4.2) for $z \ll z_N$. It is readily shown that

$$f \sim \zeta^{1/2} - \tfrac{2}{3}\lambda, \tag{4.7a}$$

$$\vartheta \sim \frac{\Theta \operatorname{erfc}\{\frac{1}{2}(|\xi| - f) - \lambda\}}{\operatorname{erfc}(-\lambda)} \qquad (|\xi| \geqslant f) \tag{4.7b}$$

$$\vartheta \sim 1 - \frac{(1-\Theta)\operatorname{erfc}\{\frac{1}{2}(f - |\xi|) + \lambda\}}{\operatorname{erfc}\lambda} \qquad (|\xi| \leqslant f) \tag{4.7c}$$

as $\zeta \to \infty$. The remaining boundary conditions are $\vartheta(\pm f, \zeta) = \Theta$ and $\vartheta \to 0$ as $|\xi| \to \infty$. Equations (4.6) can then be integrated numerically using, for example, a linearized Crank–Nicholson scheme for ϑ with the coefficients evaluated at the half-step and a second-order Runge–Kutta scheme for f. Such a scheme is second-order in both ξ and ζ. (When Θ and S are both very small, corresponding to large amounts of initial melting, there is a small region in which $f > (2\zeta)^{1/2}$ and (4.6*a*) must be integrated in the $+\zeta$ direction; the solution in this region must be matched iteratively at the singular points of (4.6*a*) to the rest of the solution.)

The similarity solutions shown in figure 7 for $\Theta = 0.25$ and $\Theta = 0.75$ with $S = 1$ are typical. In all solutions the flow is completely frozen in a region $0 \leqslant \zeta \leqslant \zeta_S(S, \Theta)$, where

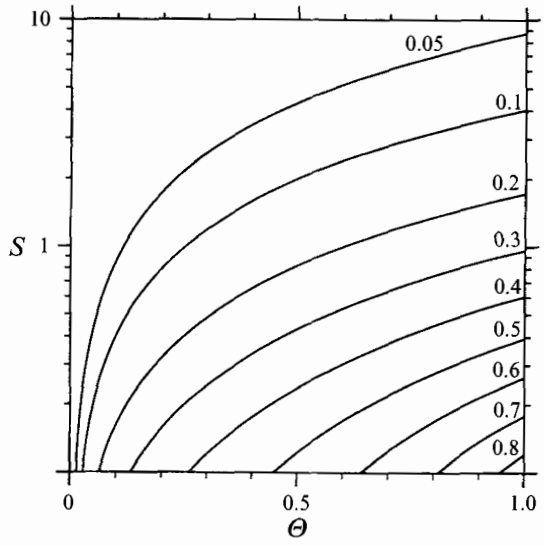

FIGURE 8. Contours of $\zeta_S^{1/2}$ as a function of S and Θ for the near-source solution (4.6). Solidification is inhibited by large Stefan number or large superheat $1-\Theta$.

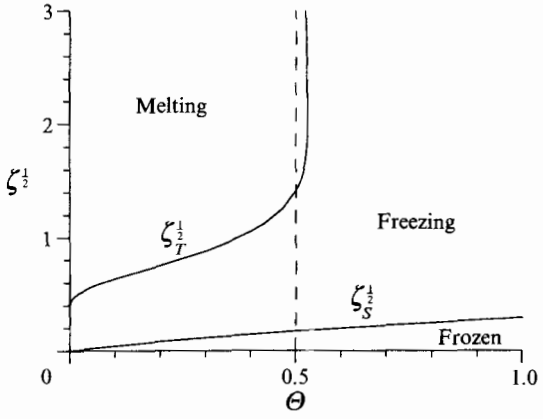

FIGURE 9. Regions of melting and solidification for near-source solutions to (4.6) for $S = 1$ and varying Θ. The transition ζ_T between melting and solidification asymptotes to $\Theta = \frac{1}{2}$ (dashed) as $\zeta \to \infty$. If $\frac{1}{2} < \Theta < 0.526$ there is a finite region in which melting occurs owing to sharpening of temperature gradients in the fluid by the flow.

$\zeta_S(S, 1) = \frac{2}{3}\lambda^2$ from §3.2. Contours of ζ_S are shown in figure 8. From the similarity scalings $c \propto z^{1/4}$ in the completely frozen region.

When $\Theta = 0.75$ the flow is solidifying everywhere. When $\Theta = 0.25$ there is a transition point $\zeta_T(S, \Theta)$ between melting far from the source and solidification close to the source. At a fixed value of z there is thus an initial period of melting after the hot flow arrives, but a later period of solidification as the finite thermal energy of the flow is depleted. The regions of melting and solidification for the near-source similarity solution are shown in figure 9 for $S = 1$. Whether there is melting or solidification as $\zeta \to \infty$ depends on whether $\Theta < \frac{1}{2}$ or $\Theta > \frac{1}{2}$. Interestingly, if $\frac{1}{2} < \Theta < 0.526$ there is a finite region in which melting occurs. At a fixed value of z in this case, there is an initial period of solidification as the hot flow is placed next to the cold boundary, a

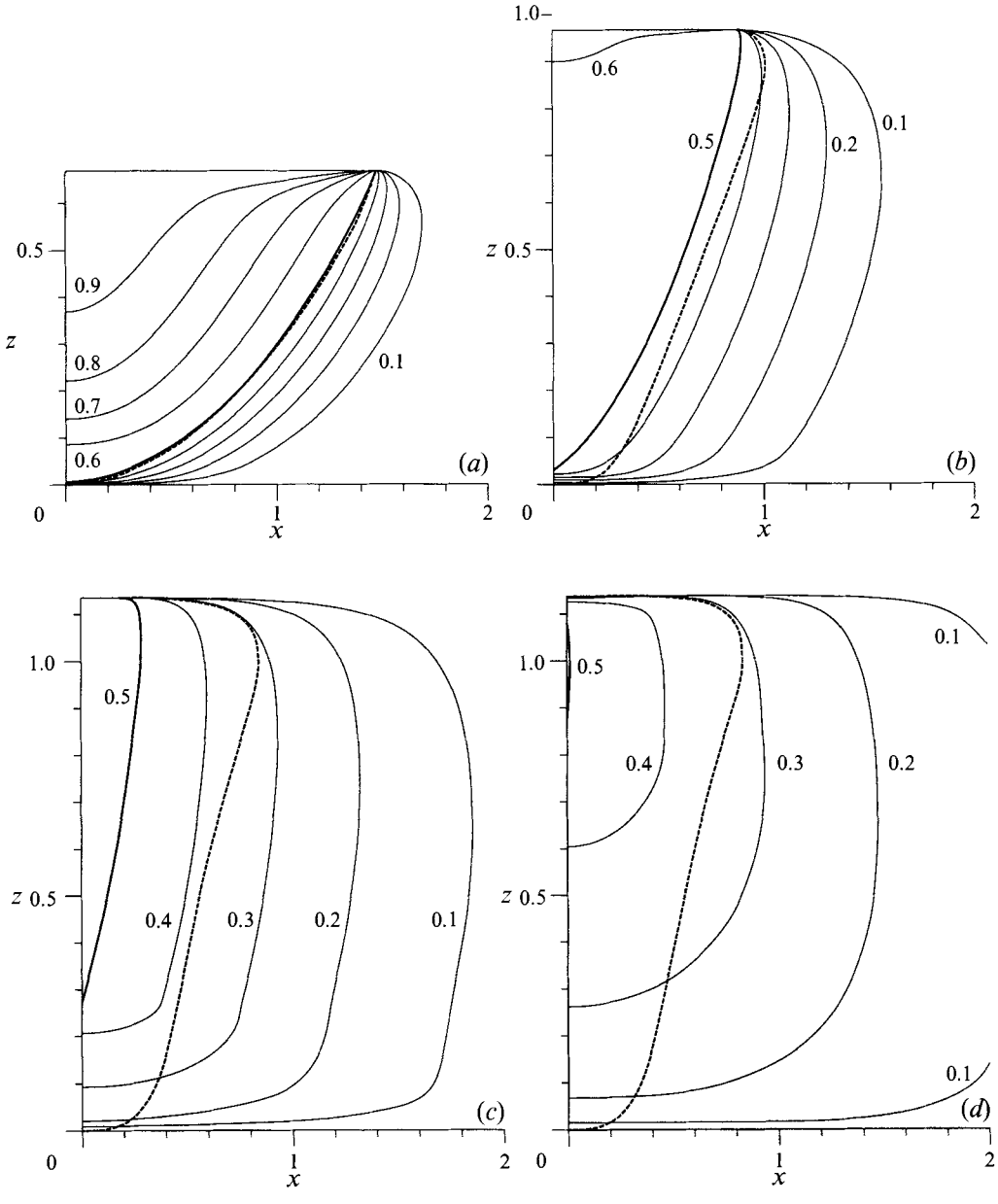

FIGURE 10. Contours of temperature θ in the solution for $S = 1$ and $\Theta = \frac{1}{2}$ at various times. The edge of the flow (bold) corresponds to the isotherm $\theta = 0.5$; the extent of the deformation $h = w + c$ is shown dashed. (*a*) By $t = 0.3$ advection has substantially distorted the thermal boundary layer in the fluid; (*b*) by $t = 1.0$ most of the superheat in the fluid has been lost; (*c*) at $t = 3.0$ the nose of the flow is nearly completely solidified; (*d*) at $t = 5.0$ the entire flow is nearly solidified.

subsequent period of melting as the temperature gradient in the fluid region is steepened by the straining component of the fluid velocity, and a final period of solidification as the thermal energy of the flow is exhausted.

4.3. *Numerical solution*

While we have been able to analyse the initial evolution of the flow and the similarity structure near the source, the full evolution of the flow must be determined numerically. An important part of the solution is treatment of the free boundaries $z = z_N(t)$ and $x = w(z, t)$. The spatial variables in the equations of heat and mass transport (2.17)–(2.19) are transformed to $(\bar{x}, \bar{z})$ by

$$\bar{x} = x/w \quad (x < w), \qquad \bar{x} = 1 + x - w \quad (x > w), \tag{4.8a, b}$$

$$\bar{z} = 1 - (1 - z/z_N)^{1/2}. \tag{4.8c}$$

This transformation maps the flow onto the rectangular domain $0 < \bar{x} \leqslant 1$, $0 \leqslant \bar{z} \leqslant 1$ and also stretches the region near $z = z_N$ in order to resolve the square-root singularities there. Where $w = 0$ the boundary condition at $\bar{x} = 1$ is changed from (2.20) to $\theta_{x+} = 0$ and the temperature is set to be uniform in $\bar{x} < 1$. The initial conditions for the calculation were determined from the short-time asymptotics.

The transformed equations for w, c and the advective terms for θ are hyperbolic with the direction of propagation being $+\bar{z}$ for w and for θ in the rapid parts of the flow and $-\bar{z}$ for c and for θ in the slower parts of the flow and the solid region. Accordingly, $\bar{z}$-derivatives were discretized using a flux-conservative Lax–Wendroff scheme. The cross-stream derivatives in the transformed equation for θ are still diffusive in character and were represented using a Crank–Nicholson discretization. Nonlinear coefficients were evaluated at a half-step in order to obtain a final scheme that was second order in both time and space. The accuracy of the calculations was tested by conservation of energy, by comparison with the asymptotic and liquidus solutions, and by grid-doubling.

The effects of the superheat $1 - \Theta$ are most important in the early stages of the flow. If Θ is less than about 0.5 then there will initially be regions of melting in the flow (cf. (4.3*d*) and figure 9). However, as the flow extends and thins, the superheat is soon lost to the surrounding solid and the flow increasingly resembles the solution for a flow with $\Theta = 1$. Zones of complete solidification spread first from the source, then from the nose of the flow and finally the whole flow is brought to rest. The evolution of the flow for the case $S = 1$, $\Theta = \frac{1}{2}$ is shown in figure 10. Owing to the superheat, the flow propagates further and for longer than the $\Theta = 1$ solution and the shape of the final solidified deposit is markedly more asymmetric (cf. figures 5*a* and 10*d*).

The time t_{max} until final solidification and the total distance propagated z_{max} depend strongly on Θ and S and each increases from zero at $(S, \Theta) = (0, 1)$ to infinity as $\Theta \to 0$ or $S \to \infty$. For example, t_{max} varies by three orders of magnitude between $(S, \Theta) = (\frac{1}{10}, 1)$ and $(S, \Theta) = (10, \frac{1}{10})$. Much of this variation can be scaled out by comparison with the simple approximation in which the superheat is neglected. We observe that if the initial temperature of the fluid were Θ rather than 1 then the evolution of the flow would be described by the analysis of §3, but with λ calculated from a rescaled Stefan number S/Θ. Accordingly we rescale the numerical results by

$$T_{max} = t_{max}[\lambda(S/\Theta, 1)]^{6/5}, \quad Z_{max} = z_{max}[\lambda(S/\Theta, 1)]^{2/5}. \tag{4.9}$$

The rescaled values are shown in figure 11.

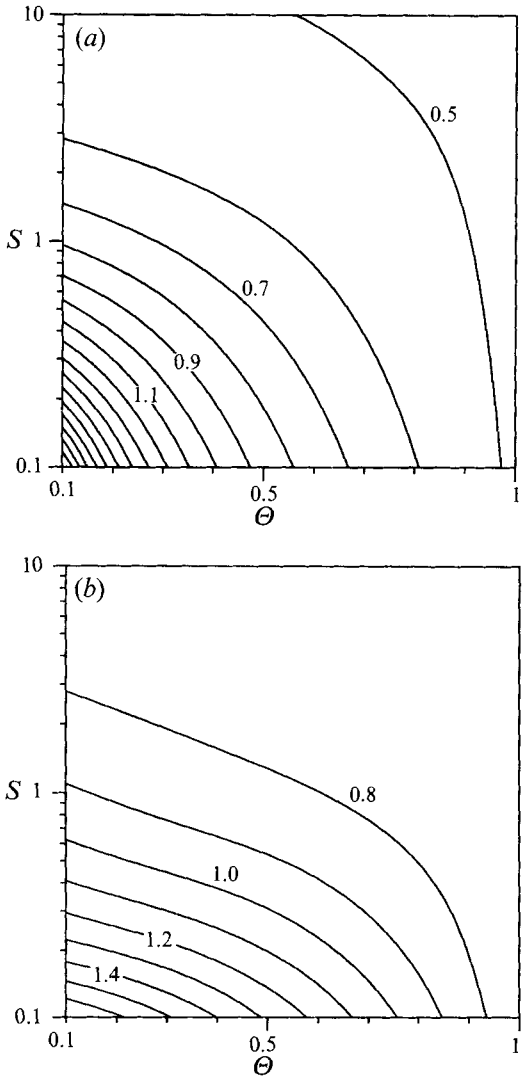

FIGURE 11. Contours of (*a*) the scaled final propagation distance Z_{max} and (*b*) the solidification time T_{max} as functions of S and Θ. The liquidus solution $Z_{max} = 0.48$ and $T_{max} = 0.72$ are good approximations if $S \gg 1-\Theta$ but significantly underestimate the true values if both S and Θ are small.

If $\Theta = 1$ then the results $T_{max} = 0.72\ldots$ and $Z_{max} = 0.48\ldots$ from §3 are exact. Indeed, these values provide good approximations provided the latent heat S is much greater than the superheat $1-\Theta$. Even if the latent heat is only twice the superheat the true values of T_{max} and Z_{max} are underestimated by no more than 20% and 30% respectively. This approximation is particularly useful since it avoids the need to recompute the full solution to the problem for particular values of S and Θ.

5. Discussion

In this paper we have analysed an example of a hot flow invading a cold environment. While the problem under discussion was motivated by a particular geological application to the propagation of magma-filled fractures in the Earth's

lithosphere, similar analytical techniques and ideas will apply to more general problems. Long thin flows can, as might be expected, be described by lubrication theory for both the heat and mass transport. However, the analysis is complicated by two novel features which arise in propagation into a cold environment. Firstly, the thermal evolution is influenced by the conditions both at the nose and at the origin of the flow so that the information transport in the heat equation is bidirectional (as in heat-exchanger problems); the upstream and downstream influences are coupled by cross-stream diffusion and cannot be solved for separately. Secondly, the equation for the propagation velocity of the frontal shock must be augmented by heat-conservative boundary conditions on the temperature at the nose of the flow.

A number of asymptotic results have been obtained for a buoyancy-driven, fixed-volume, two-dimensional flow between flexible boundaries. The boundary-layer analysis of §4.1 shows that the initial effects of solidification (melting) are to retard (advance) the position of the nose from the kinematic-wave solution (in which $z_N \propto t^{1/3}$) by an amount proportional to $t^{7/6}$. Higher-order corrections may be developed as a regular perturbation series (Appendix B). Near the origin, the flow is self-similar and solidifies completely in a zone of length initially proportional to t^2 (§§3.2 and 4.2). In each case, if the fluid is initially at its liquidus temperature then the analysis is considerably simplified and can be generalized to turbulent flows.

If the fluid temperature is initially above the liquidus then the interaction of advection, diffusion and latent-heat release can produce complex patterns of solidification and melting. At a given position it is possible to observe only solidification, or melting and then solidification, or even solidification then melting and then solidification again, depending on whether the dimensionless solidification temperature $\Theta = (T_L - T_\infty)/(T_0 - T_\infty)$ is much greater than $\frac{1}{2}$, less than $\frac{1}{2}$, or just greater than $\frac{1}{2}$. In rough terms, the flow will initially melt or solidify if $\Theta < \frac{1}{2}$ or $\Theta > \frac{1}{2}$. Eventually, however, the flow will always solidify if $\Theta > 0$, with complete solidification proceeding first from the origin and then also from the nose of the flow.

From a geological standpoint, the most significant observation is that solidification brings the flow to rest after a finite time and distance of propagation. The calculation thus provides a quantitative demonstration that the penetration of dykes through the lithosphere can be limited by thermal effects as well as by any level of neutral buoyancy. The solutions given allow the final distance and time of flow and the shape of the solidified deposit to be evaluated. In dimensional terms the extent of flow is given by

$$z_{max} = Z_{max}(S, \Theta)\left(\frac{(\frac{3}{4}Q)^4 (g\Delta\rho/\mu)}{\kappa\lambda(S^*)^2}\right)^{1/5} \tag{5.1a}$$

$$t_{max} = T_{max}(S, \Theta)\left(\frac{(\frac{3}{4}Q)^2}{(g\Delta\rho/\mu)^2 (\kappa\lambda(S^*)^2)^3}\right)^{1/5}, \tag{5.1b}$$

where $S^* = S/\Theta$, $\lambda(S^*)$ is the root of (3.3c), and the coefficients Z_{max} and T_{max} are given either by figure 10 or, if $S \gg 1-\Theta$, by the approximations 0.48 and 0.72.

The geological values of the parameters in (5.1) vary widely but, as an illustrative example of a basaltic dyke, we take $\Delta\rho = 300$ kg m^{-3}, $\mu = 100$ Pa s, $Q = 10^4$ m^2, $C_p = 10^3$ J kg^{-1} °C^{-1}, $L = 4 \times 10^5$ J kg^{-1}, $\kappa = 10^{-6}$ m^2 s^{-1}, $T_0 = 1250$ °C, $T_L = 1200$ °C and $T_\infty = 400$ °C (e.g. Bruce & Huppert 1989; Spence & Turcotte 1990). Hence $S = 0.47$, $\Theta = 0.94$, $\lambda(S^*) = 0.54$ and we calculate that $z_{max} = 21$ km and $t_{max} = 15$ hours, corresponding to a final average width of 0.5 m. If the dyke intersects the Earth's surface then the proportion of magma erupted is given by figure 5(b).

A further observation of geological significance is that the shape of the final solidified product (e.g. figures 5*a*, 10*d*) does not reflect either the active region of flow at any time, or the static equilibrium of a fluid that solidifies post-emplacement. Thus the field geologist, whose only observation is often the solidified flow, may find it difficult to infer either the dimensions of the active flow or the dynamics of emplacement.

The techniques developed herein are readily applied to a range of further problems. In the companion paper to this (Lister 1994) we examine the case of continual input of hot fluid and determine the conditions under which propagation will ultimately cease. It would be of interest to extend the calculations to unequal solidification temperatures of the initial solid and fluid, which would be expected to lead to a further order of complexity in the pattern of melting and solidification (cf. Huppert 1989). For lava flows, the convective or radiative heat transfer to the environment is relatively rapid (Fink & Griffith 1990) and the heat loss is limited by conduction through the solidified skin of the flow. In this case, lava flows with a thin flexible skin can be described by analysis similar to the above in which the fixed temperature condition at infinity is replaced by a fixed temperature condition at the outer margin of the chill. Alternatively, the effects of convection or radiation can be retained by use of an appropriate heat-flux condition on the margin of the chill. Such problems will form the basis of future investigations.

I am grateful to R. C. Kerr and H. E. Huppert for constructive comments on an earlier version of this manuscript.

Appendix A. Turbulent flows

We have noted that if the temperature of the fluid is initially on the liquidus ($\Theta = 1$) then the fluid remains at a uniform temperature $\theta = 1$ for the duration of the flow. This allows us to extend the theory developed in §3, firstly to turbulent flows and secondly to higher-order terms in the short-time expansion.

In the laminar regime the flux driven by the pressure gradient $\partial p/\partial z = -\Delta\rho g$ is

$$q = (2\Delta\rho g/3\mu)\, w^3. \tag{A 1}$$

If the Reynolds number $Re = \rho_f q/\mu$ exceeds $O(10^3)$ then the flow will be turbulent rather than laminar and the flux will be given by an appropriate empirical flow law. As discussed by Lister (1990*a*), two popular suggestions for the flow law are

$$q = 15.4[(\Delta\rho g)^4/\mu\rho_f^3]^{1/7}\, w^{12/7}, \tag{A 2}$$

$$q = (8\Delta\rho g/k\rho_f)\, w^{3/2}, \tag{A 3}$$

where k is a friction factor, each of which has some theoretical and experimental support (Schlichting 1968; Hirs 1974). Accordingly, we assume that in appropriate dimensionless variables the flow law takes the form

$$q = w^{n+1}/(n+1), \tag{A 4}$$

where (A 1)–(A 3) correspond to $n = 2$, $\frac{5}{7}$ and $\frac{1}{2}$ respectively.

As in §3, the thermal evolution is described by an error-function profile in the solid. The remaining equations are

$$w_t + w^n w_z = -\frac{\lambda}{[t - t_N(z)]^{1/2}} \quad (w > 0), \tag{A 5}$$

$$\mathrm{d}z_N/\mathrm{d}t = w_N^n/(n+1), \tag{A 6}$$

n	Z_{max}	T_{max}
$\frac{1}{2}$	0.409	0.481
$\frac{5}{7}$	0.426	0.539
1	0.445	0.604
2	0.483	0.715

TABLE 1. The dimensionless solidification times and distances for a flow at its liquidus temperature which obeys a flux law $q \propto w^{n+1}$

with initial conditions

$$\lim_{t\to 0_+} \int_0^{z_N(t)} w(z,t)\,\mathrm{d}z = \frac{n}{n+1}, \quad \lim_{t\to 0_+} z_N(t) = 0. \tag{A 7a, b}$$

The parameter λ may be removed by the rescalings

$$Z = z\lambda^{2/(n+3)}, \quad W = w\lambda^{-2(n+3)}, \quad T = t\lambda^{2(n+1)/(n+3)}, \tag{A 8}$$

and the rescaled equations solved by the method of characteristics. The solidification times and distances corresponding to (A 1)–(A 3) are given in table 1.

The near-source behaviour can be analysed as in §3.2 to show that

$$Z(T) = \int_0^T \{W(T) + 2T^{1/2} - 2\tau^{1/2}\}^n \,\mathrm{d}\tau. \tag{A 9}$$

It follows that $W = T^{1/2}F(Z/T^{1+n/2})$, where

$$\{F(\eta)+2\}^{n+2}\,\beta\left(\frac{2}{F(\eta)+2}; 2, n+1\right) = 2\eta, \tag{A 10}$$

and the incomplete beta function is defined by

$$\beta(V; a, b) = \int_0^V v^{a-1}(1-v)^{b-1}\,\mathrm{d}v. \tag{A 11}$$

Hence the zone of complete solidification near the source is given asymptotically by

$$Z_S = \frac{2^{n+1}T^{1+n/2}}{(n+1)(n+2)}. \tag{A 12}$$

Appendix B. Short-time expansions

A higher-order short-time expansion of (A 5)–(A 7) is better developed as an expansion in powers of $\phi = \lim_{t\to 0} W^n$ than of λ. Let $T_N(\phi)$ and $Z_N(\phi)$ denote the time and position that the characteristic ϕ reaches the front. We define a stretched time variable by $\tau(\phi) = T/T_N(\phi)$ in order to fix the front at $\tau = 1$. Thus (A 5) may be integrated along a characteristic to yield

$$W(\tau;\phi) = \phi^{1/n} - T_N(\phi)^{1/2} \int_0^\tau \frac{\mathrm{d}v}{[v - T_N(\phi_N[Z(v;\phi)])/T_N(\phi)]^{1/2}}, \tag{B 1}$$

where $\phi_N(Z)$ is the inverse of $Z_N(\phi)$.

We now introduce $\epsilon = \phi^{-(n+3)/2n}$ and expand the unknowns by

$$\phi^{1/n} Z(\tau;\phi) = Z^*(\tau;\epsilon) = Z_0(\tau) + \epsilon Z_1(\tau) + \ldots, \tag{B 2a}$$

$$\phi^{(n+1)/n} T_N(\phi) = T_N^* = T_0 + \epsilon T_1 + \ldots, \tag{B 2b}$$

$$\phi_N(Z) = Z^{-n}(\phi_0 + \phi_1 Z^a + \phi_2 Z^{2a} + \ldots) = \phi Z^{*-n}(\phi_0 + \phi_1 \epsilon Z^{*a} + \phi_2 (\epsilon Z^{*a})^2 + \ldots), \tag{B 2c}$$

where $a = \frac{1}{2}(n+3)$. From (B 1) the equation defining a characteristic and (A 6) may be written as

$$\frac{\partial Z^*}{\partial \tau} = T_N^* \left(1 - \epsilon T_N^{*1/2} \int_0^\tau \frac{\mathrm{d}v}{[v - T_N(\phi_N[Z])/T_N(\phi)]^{1/2}}\right)^n, \tag{B 3a}$$

$$(n+1)\frac{\mathrm{d}Z(1;\phi)}{\mathrm{d}\phi} = \left(\phi \frac{\mathrm{d}T_N}{\mathrm{d}\phi}\right)\left(1 - \epsilon T_N^{*1/2} \int_0^1 \frac{\mathrm{d}v}{[v - T_N(\phi_N[Z])/T_N(\phi)]^{1/2}}\right)^n \tag{B 3b}$$

respectively, and we also have the identity

$$\phi_N[Z(1;\phi)] = \phi. \tag{B 3c}$$

Substitution of (B 2) into (B 3) yields a series of equations at successive powers of ϵ which determines the coefficients $Z_i(\tau)$, T_i and ϕ_i. The expansion is regular (unlike the expansion in powers of λ) and can be taken to arbitrary order.

The leading-order coefficients that satisfy (A 7*a*) are

$$Z_0 = \tau, \quad T_0 = \phi_0 = 1. \tag{B 4}$$

At order ϵ^1, a little algebra produces

$$Z_1(\tau) = T_1 \tau - n \int_0^\tau \int_0^{\tau'} \frac{\mathrm{d}v\,\mathrm{d}\tau'}{(v - v^{n+1})^{1/2}} = T_1 \tau - \beta\left(\tau^{1/n}; \frac{1}{2}, \frac{1}{2n}\right)\tau + \beta\left(\tau^{1/n}; \frac{1}{2}, \frac{3}{2n}\right), \tag{B 5a}$$

$$T_1 = \frac{n+1}{n}\left(\mathrm{B}\left(\frac{1}{2}, \frac{1}{2n}\right) - \frac{5+n}{3+n}\mathrm{B}\left(\frac{1}{2}, \frac{3}{2n}\right)\right), \tag{B 5b}$$

$$\phi_1 = nZ_1(1) = \mathrm{B}\left(\frac{1}{2}, \frac{1}{2n}\right) - \frac{5+3n}{3+n}\mathrm{B}\left(\frac{1}{2}, \frac{3}{2n}\right). \tag{B 5c}$$

Hence

$$T_N(\phi_N(Z)) = Z^{n+1}\left(1 + \frac{2(n+1)}{n+3}\mathrm{B}\left(\frac{1}{2}, \frac{3}{2n}\right) Z^a + O(Z^{2a})\right), \tag{B 6a}$$

$$Z_N(T) = T^{1/(n+1)}\left(1 + \frac{2}{n+3}\mathrm{B}\left(\frac{1}{2}, \frac{3}{2n}\right) T^{(n+3)/2(n+1)} + O(T^{(n+3)/(n+1)})\right), \tag{B 6b}$$

which reduces to (3.14) when $n = 2$.

REFERENCES

Aki, K., Fehler, M. & Das, S. 1977 Source mechanisms of volcanic tremor: Fluid-driven crack models and their application to the 1963 Kilauea eruption. *J. Volcanol. Geotherm. Res.* **2**, 259–287.

Bruce, P. M. & Huppert, H. E. 1989 Thermal control of basaltic fissure eruptions. *Nature* **342**, 665–667.

Bruce, P. M. & Huppert, H. E. 1990 Solidification and melting in dykes by the laminar flow of basaltic magma. In *Magma Transport and Storage* (ed. M. P. Ryan). Wiley.

Carslaw, H. S. & Jaeger, J. C. 1959 *Conduction of Heat in Solids.* Oxford University Press.

DELANEY, P. T. 1987 Heat transfer during emplacement and cooling of mafic dykes. In *Mafic Dyke Swarms* (ed. H. C. Halls & W. H. Fahrig). Geol. Soc. Canada Special Paper 34.

DELANEY, P. T. & POLLARD, D. D. 1982 Solidification of basaltic magma during flow in a dike. *Am. J. Sci.* **282**, 856–885.

EINARSSON, P. & BRANDSDÓTTIR, B. 1980 Seismological evidence for lateral magma intrusion during the July 1978 deflation of the Krafla volcano in NE-Iceland. *J. Geophys.* **47**, 160–165.

FEDOTOV, S. A. 1978 Ascent of basic magmas in the crust and the mechanism of basaltic fissure eruptions. *Intl Geol. Rev.* **20**, 33–48.

FINK, J. H. & GRIFFITHS, R. W. 1990 Radial spreading of viscous-gravity currents with solidifying crust. *J. Fluid Mech.* **221**, 485–509.

GRADSHTEYN, I. S. & RYZHIK, I. M. 1980 *Table of Integrals, Series, and Products*. Academic.

HIRS, G. G. 1974 A systematic study of turbulent film flow. *J. Lubric. Tech.* **96**, 118–126.

HUPPERT, H. E. 1982 Flow and instability of a viscous current down a slope. *Nature* **300**, 427–429.

HUPPERT, H. E. 1989 Phase changes following the initiation of a hot turbulent flow over a cold solid surface. *J. Fluid Mech.* **198**, 293–319.

LISTER, J. R. 1990*a* Buoyancy-driven fluid fracture: similarity solutions for the horizontal and vertical propagation of fluid-filled cracks. *J. Fluid Mech.* **217**, 213–239.

LISTER, J. R. 1990*b* Buoyancy-driven fluid fracture: the effects of material toughness and of low viscosity precursors. *J. Fluid Mech.* **210**, 263–280.

LISTER, J. R. 1991 Steady solutions for feeder dykes in a density-stratified lithosphere. *Earth Planet. Sci. Lett.* **107**, 233–242.

LISTER, J. R. 1994 The solidification of buoyancy-driven flow in flexible-walled channel. Part 2. Continual release. *J. Fluid Mech.* **272**, 45–65.

LISTER, J. R. & KERR, R. C. 1991 Fluid-mechanical models of crack propagation and their application to magma-transport in dykes. *J. Geophys. Res.* **96**, 10049–10077.

MUSKHELISHVILI, N. I. 1963 *Some Basic Problems of the Mathematical Theory of Elasticity*. Noordhoff.

PASTERIS, J. D. 1984 Kimberlites: complex mantle salts. *Ann. Rev. Earth Planet. Sci.* **12**, 133–153.

POLLARD, D. D. 1976 On the form and stability of open hydraulic fractures in the Earth's crust. *Geophys. Res. Lett.* **3**, 513–516.

POLLARD, D. D. 1987 Elementary fracture mechanics applied to the structural interpretation of dykes. In *Mafic Dyke Swarms* (ed. H. C. Halls & W. H. Fahrig). Geol. Soc. Canada Special Paper 34.

POLLARD, D. D. & HOLZHAUSEN, G. 1979 On the mechanical interaction between a fluid-filled fracture and the Earth's surface. *Tectonophysics* **53**, 27–57.

SCHLICHTING, H. 1968 *Boundary-Layer Theory*. McGraw-Hill.

SECOR, D. T. & POLLARD, D. D. 1975 On the stability of open hydraulic fractures in the Earth's crust. *Geophys. Res. Lett.* **2**, 510–513.

SHAW, H. R. 1980 The fracture mechanisms of magma transport from the mantle to the surface. In *Physics of Magmatic Processes* (ed. R. B. Hargreaves), pp. 201–264. Princeton.

SPENCE, D. A., SHARP, P. W. & TURCOTTE, D. L. 1987 Buoyancy-driven crack propagation: a mechanism for magma migration. *J. Fluid Mech.* **174**, 135–153.

SPENCE, D. A. & TURCOTTE, D. L. 1985 Magma-driven propagation of cracks. *J. Geophys. Res.* **90**, 575–580.

SPENCE, D. A. & TURCOTTE, D. L. 1990 Buoyancy-driven magma fracture: a mechanism for ascent through the lithosphere and the emplacement of diamonds. *J. Geophys. Res.* **95**, 5133–5139.

SPERA, F. 1980 Aspects of magma transport. In *Physics of Magmatic Processes* (ed. R. B. Hargreaves), pp. 265–323. Princeton.

TURCOTTE, D. L. & SCHUBERT, G. 1982 *Geodynamics*. John Wiley.

WEERTMAN, J. 1971 The theory of water-filled crevasses in glaciers applied to vertical magma transport beneath oceanic ridges. *J. Geophys. Res.* **76**, 1171–1183.

WILSON, L. & HEAD, J. W. 1981 Ascent and eruption of basaltic magma on the Earth and Moon. *J. Geophys. Res.* **86**, 2971–3001.